Effect of pH on the Activity of Ice-Binding Protein from *Marinomonas primoryensis*

*Elizabeth A. Delesky [1], Patrick E. Thomas [2,3], Marimikel Charrier [4], Jeffrey C. Cameron [2,3,5], and Wil V. Srubar III [1,4,]**

[1] Materials Science and Engineering Program, University of Colorado Boulder, Boulder, CO 80309, USA; elizabeth.delesky@colorado.edu (E.A.D.)
[2] Department of Biochemistry, University of Colorado Boulder; Boulder, CO 80303, USA; patrick.thomas@colorado.edu (P.E.T.)
[3] Renewable and Sustainable Energy Institute, University of Colorado, Boulder, CO 80309, USA; jeffrey.c.cameron@colorado.edu (J.C.C.)
[4] Department of Civil, Environmental, and Architectural Engineering, University of Colorado Boulder, Boulder, CO 80309; mmcharrier@colorado.edu (M.C.)
[5] National Renewable Energy Laboratory, Golden, CO 80401, USA * Correspondence: wsrubar@colorado.edu (W.V.S.III); Tel.: +1-303-492-2621

Abstract: The ability of an ice-binding protein (IBP) from *Marinomonas primoryensis* (*Mp*IBP) to influence ice crystal growth and structure in non-physiological pH environments was investigated in this work. The ability for *Mp*IBP to retain ice interactivity under stressed environmental conditions was determined *via* (1) a modified splat assay to determine ice recrystallization inhibition (IRI) of polycrystalline ice and (2) nanoliter osmometry to evaluate the ability of *Mp*IBP to dynamically shape the morphology of a single ice crystal. Circular dichroism (CD) was used to relate the IRI and DIS activity of *Mp*IBP to secondary structure. Results illustrate that *Mp*IBP secondary structure was stable between pH 6 – pH 10. It was found that *Mp*IBP did not interact with ice at pH ≤ 4 or pH ≥ 13. At 6 ≤ pH ≥ 12 *Mp*IBP exhibited a reduction in grain size of ice crystals compared to control solutions and demonstrated dynamic ice shaping at 6 ≤ pH ≥ 10. The results substantiate that *Mp*IBP retains some secondary structure and function in non-neutral pH environments, thereby enabling its potential utility in non-physiological materials science and engineering applications.

Keywords: ice-binding proteins; antifreeze proteins; pH; ice recrystallization inhibition; dynamic ice shaping

1. Introduction

Previous research indicates that ice-binding proteins (IBPs) may offer an alternative to conventional frost-prevention strategies for biological cryopreservation (Davies 2014; Liang 2016) and, by extension, antifreeze applications in a host of other commercial industries such as coolants in aerospace engineering, frost-resistant pavements in civil engineering, and anti-icing coatings for energy infrastructure such as solar panels or wind turbines. While IBPs offer a promising biological solution for these ice-growth prevention applications, proteins are well known to unfold, refold,

denature, aggregate, or degrade in non-physiological environments (Ptitsyn 1987). Applications with harsh chemical environments, such as concrete in civil engineering that has a pore solution pH of 12-13 (Ghods 2009), would benefit from a material that inhibits ice recrystallization. Freeze-thaw damage in concrete is due, in part, to the expansion of ice crystals (Powers 1975) demonstrating a need for materials that inhibit ice growth in extreme pH environments. To the authors' knowledge, some studies have investigated the effect of pH on thermal hysteresis activity (Chao 1994; Gauthier 1998; Kristiansen 2005; Li 1998; Wu 1991), and a limited number of studies have indicated that IBPs may produce similar ice recrystallization inhibition (IRI) activity in non-physiological pH solutions (Leiter 2016; Delesky 2019) which necessitates pH studies for the IRI activity of IBPs in non-physiological environments.

IBPs are a diverse category of proteins that have evolved independently among many types of organisms, including plants (Duman 1993; Griffith 1992; Middleton 2014; Moffatt 2006), fungi (Duman 1993; Hoshino 2003; Xiao 2010), fish (Davies 1988; DeVries 1988; Fletcher 1987; Hew 1981; Marshall 2004; Slaughter 1981), insects (Graether 2000; Graham 2005; Liou 1999), and microbes (Duman 1993; Garnham 2008; Gilbert 2004; Vance 2018) to help them survive in freezing environments. As IBPs come from a wide range of organisms, they vary in molecular weight, structure, and activity (Bar-Dolev 2016b). X-ray crystallography and NMR studies have resolved IBP structures to include α-helices, β-solenoids, helix bundles, and small globular proteins (Bar-Dolev 2016b). Although all structures exhibit the ability to adsorb to ice, there are few trends among residues or sequences that lead to ice binding (Bar-Dolev 2016b). Mechanistically, the current hypothesis for IBP function is through adsorption-inhibition (Bar-Dolev 2016b). The ice-binding face of an IBP is composed of regularly spaced ice-binding residues that match the lattice spacing of one or more faces of the ice crystal lattice. The lattice match allows the protein to adsorb to a nascent ice crystal and induce high local curvature on the ice crystal surface that makes further crystal growth energetically unfavorable, a phenomenon known as the Gibbs-Thomson effect (Bar-Dolev 2016b; Graether 2000; Jia 1996; Knight 1991; Liou 2000). All IBPs exhibit one or more phenomena that indicate their interaction with ice. These phenomena include: (1) thermal hysteresis (TH), a non-colligative depression of freezing-point temperature while maintaining (or raising) the melting point; (2) dynamic ice shaping (DIS), a reshaping of the 1H hexagonal ice structure to form less disruptive ice geometries; and (3) ice recrystallization inhibition (IRI), a property that limits ice recrystallization through Ostwald ripening and overall reduces mean crystal size (Voets 2017). *Marinomonas primoryensis* is an Antarctic bacterium that uses a 1.5 MDa extracellular protein to keep it in the oxygen and nutrient rich phototropic zone by binding to the surface of ice (Bar-Dolev 2016a; Bar-Dolev 2016b). Of the 1.5 MDa protein, a 34 kDa region, dubbed region IV, is responsible for ice-binding (Bar-Dolev 2016a). The ice-binding region consists of mostly β-strands that form a calcium-stabilized β-solenoid (Garnham 2008; Vance 2014). The β-solenoid structure of the *Marinomonas primoryensis* IBP is similar to other hyperactive IBPs, though few IBPs have calcium

stabilized structures. The calcium-stabilization offers a unique potential for a more robust structure in non-ideal environments.

The purpose of this work was to investigate the ability of the calcium-stabilized ice-binding region IV from the *Marinomonas primoryensis* extracellular adhesion protein (*Mp*IBP) to control the size and inhibit the growth of ice crystals in non-physiological pH solutions ($2 \leq pH \geq 13$). It is not known whether the calcium-stabilized *Mp*IBP is also pH tolerant, thus, we characterized its activity in non-physiological solutions.

2. Materials and Methods

2.1. Materials

All reagents were purchased from Fisher Bioreagents without further purification. Clonal cells with *Mp*IBP were obtained from Dr. Peter Davies at Queen's University in Kingston, Ontario, Canada and used for protein expression (Garnham 2008). Solutions with a pH range from 2 to 13 were created at room temperature in increments of ~2 by adding HCl to create acidic solutions and adding NaOH to create basic solutions, and pH was measured again at 0 °C (Table 1). *Mp*IBP at each pH was compared to its respective control pH solution so that all constituents were the same save for the addition of *Mp*IBP. pH 8 was used as the reference solution as it was close to the pH of purification solutions (~8.5). Tris(hydroxymethyl)aminomethane (Tris) was carried over from protein purification and therefore included in control solutions to account for protein addition. Total ionic strength (I) for each solution was calculated according to Equation (1):

$$I = \frac{1}{2}\sum Z^2 C, \quad (1)$$

where Z is the valence of the ion and C is the concentration. Varied pH solutions were tested for IRI and DIS either as a control or loaded with 0.1 mg/ml *Mp*IBP. A protein concentration of 0.1 mg/ml was used in this study as this was previously determined to be the level at which *Mp*IBP thermal hysteresis activity is at a maximum (Garnham 2008). It was anticipated for *Mp*IBP in pH 4 solution the concentration might have been less than 0.1 mg/ml as pH 4 is close to the isoelectric point of 4.11 (Table S1), which often reduces protein solubility (Xia 2018). The concentration of *Mp*IBP in pH 4 solution was lower than 0.1 mg/ml and measured using UV-Vis at 280 nm and was found to be ~0.04 mg/ml (Table S2). Table S3 provides the composition for solutions used during *Mp*IBP production and purification procedures.

Table 1 Solutions for evaluating *Mp*IBP efficacy in different pH conditions

pH			Constituents (mM)					Total Ion Content		
Target	**Ambient**	**0 °C**	**Tris**	**NaCl**	**$CaCl_2$**	**NaOH**	**HCl**	**Na^+ (mM)**	**Cl^- (mM)**	***I* (mol/L)**
2	2.15	3.31	10	15	10	-	32	15	67	0.066
4	3.99	5.81	10	15	10	-	25	15	60	0.063

6	6.18	6.93	10	15	10	2.6	26	17.6	61	0.064
8	8.06	9.21	10	15	10	-	8.5	15	43.5	0.054
10	9.98	10.52	10	15	10	8.4	2.5	23.4	37.5	0.055
12	12.01	13.08	10	15	10	44	-	59	35	0.078
13	12.98	*14+	10	15	10	219	-	234	35	0.207

*Measured pH was above the threshold of the pH meter

2.2. Expression of MpIBP

Expression of *Mp*IBP was adapted from Garnham *et al.* (2008). Briefly, a culture was used to inoculate 1.6 L of lysogeny broth (LB) medium with kanamycin (100 μg/mL) and grown until OD_{600} reached 0.5 (37 °C, 200 rpm). The temperature was lowered to 23 °C until cells reached $OD_{600} = 1$ (~2 hours). Then, isopropyl β-D-1-thiogalactopyranoside was added to a final concentration of 1 mM to induce expression overnight. Cells were recovered by centrifugation (30 min, 4,300 g, 4 °C), resuspended in Buffer A (Table S2), and lysed using a Qsonica Q55 Sonicator Ultrasonic Homogenizer with Probe 55W (5x, 45 seconds, 50% amplitude). Cellular debris was removed *via* centrifugation (1.5 hours, 4 °C, 4,300 g) on a Beckman Coulter Allegra X-14R Centrifuge with a SX4750A rotor.

2.3. Purification of MpIBP

The cellular supernatant was mixed with 16 mL of Ni-NTA (Ni^{2+}-nitriloacetate) resin (16 hr, 4 °C), loaded into a column, washed with Buffers A through C, and eluted with Buffers D and E (Table S2). Fractions were examined using SDS-PAGE, and samples displaying bands for *Mp*IBP (~34kD) were pooled before running through a ThermoScientific Protein Biology 50 mL 30kD Pierce Protein Concentrator (2000g, 4 °C) in Buffer F (10-fold reduction, 3x). The concentrate was loaded onto a DEAE–Sepharose resin column equilibrated with Buffer F, washed with Buffers F through H, and protein was eluted using Buffers I through K (Table S2). Fractions displaying a band for *Mp*IBP *via* SDS-PAGE were pooled and concentrated, then run on a GE Healthcare AKTApurifier FPLC with a Frac 950 equipped with a HiLoad Superdex 75 PG preparative size exclusion chromatography column. Fractions that displayed a band for *Mp*IBP *via* SDS-PAGE were again pooled and concentrated. Concentrate purity was verified using SDS-PAGE (Fig. S1), and absorbance at 280 nm. The final yield was 3 mg of pure *Mp*IBP.

2.4. Blue Native Polyacrylamide Gel Electrophoresis (BN-PAGE)

Blue-native polyacrylamide gel electrophoresis (BN-PAGE) was performed on *Mp*IBP in varied pH solutions at a concentration of 0.4 mg/ml to ensure visible bands in the gel. BN-PAGE procedures were adapted from Fiala *et al.* (2011) and Krause *et al.* (2008). Briefly, protein solutions were stained using sample buffer (50 mM bis-tris, 5% w/v Coomassie brilliant blue, 10% glycerol, pH 7). Samples were dry-loaded into a 10% denaturing acrylamide gel (1.75 mm x 10 well; 80 min, 300 mA; outer

buffer 1X Tris-Glycine Native PAGE running buffer, pH 8.3) and run using a voltage of 100 V until the samples entered the separating gel, where the voltage was increased to 150 V. Samples were compared to a 10-250 kDa PageRuler Plus protein ladder (ThermoFisher Scientific) to estimate molecular weight. *Mp*IBP content within the gel was stained using Coomassie SimplyBlue SafeStain (Invitrogen) according to manufacturer specifications.

2.5. Size-Exclusion Chromatography with Multi-Angle Light Scattering Detector (SEC-MALS)

Varied pH solutions were analyzed as controls or loaded with 1 mg/ml *Mp*IBP using size-exclusion chromatography (SEC) equipped with a multi-angle light scattering (MALS) detector. SEC was performed on an Agilent 1100 Series LC system and a Tosoh TSKgel G3000SWxl size exclusion column. MALS was performed using a Wyatt miniDAWN Treos II. The mobile phase was 30 mM tris, 150 mM NaCl, and 10 mM $CaCl_2$ at a flow rate of 0.4 mL/min. 50 µL of each sample were analyzed (50 µg *Mp*IBP/injection). Data were processed using Astra software 7.1.2 and were compared against a bovine serum albumin (BSA) standard to determine size. Data were smoothed using an FFT algorithm with a 15-point window and plotted using Origin 2019.

2.6. Circular Dichroism (CD) Spectroscopy

Circular dichroism (CD) spectra were collected on a modular Applied Photophysics Chirascan Plus CD and Fluorescence Spectrometer in the far UV range (190-260 nm) at ambient temperature with 0.5 nm steps and 0.5 sec/step at a 0.5 mm path length. *Mp*IBP was loaded at 0.4 mg/ml to ensure adequate detection of the protein. The solutions were tested from 260 nm to a varied minimum wavelength. The final wavelength was altered to be as low as possible per sample before the signal detection limits of the instrument were saturated from the interference of the pH adjusters, namely HCl and NaOH, as they absorb in the peptide bond region (Buck 1954). *Mp*IBP was incubated in solutions for at least 24 hours before testing to ensure equilibrium folding states (Song 2017).

Five repeat scans were averaged for each loading of *Mp*IBP in pH solutions and the corresponding baseline for the control pH solution. After removing the control solution baseline, noise was removed from the data in the Chirascan Software using the Savitzky-Golay smoothing filter using five points per window with a polynomial order of two. Protein conformation (% helix, strand, turns, etc.) was measured from the peptide bond region (<240 nm) (Kelly 2005) using BeStSel software (Misconai 2015) with the exception of the pH 13 sample as the measured data set did not meet the minimum wavelength range for deconvolution.

2.7. Ice Recrystallization Inhibition (IRI)

Ice recrystallization inhibition of *Mp*IBP was investigated using a splat assay adapted from Knight *et al*. (1988). Varied pH solutions were tested as controls or with a 0.1 mg/ml loading of *Mp*IBP. Splats were performed in triplicate. A 10 µL droplet of sample was dispensed from 1.7 m

through a PVC pipe onto a microscope slide on an aluminum block chilled with dry ice to obtain a single layer of ice crystals. The slide was rapidly transferred to an Otago nanoliter osmometer sample stage annealed at -4 °C for 30 min. The temperature was monitored using a bead-type thermocouple. Ice recrystallization was observed by collecting images immediately after the splat was performed (t_0) to ensure a polycrystalline sample had been obtained, and again at 30 minutes (t_{30}) to observe IRI activity. Images were taken using an Olympus BX41 microscope with an Olympus PLN 10X objective (NA = 0.25), equipped with an Axiocam 506 color camera on a 1" 1.0x 60N C-mount adapter.

2.8. Dynamic Ice Shaping (DIS)

*Mp*IBP was tested for dynamic ice shaping (DIS) in pH solutions by modifying a protocol established by Bar-Dolev et al. (2012) using an Otago nanoliter osmometer sample stage mounted on an Olympus BX41 microscope with an Olympus LUCPlanFL N 20x /0.45 Ph1 microscope objective (NA = 0.45). *Mp*IBP pH solutions were tested for DIS at a solution concentration of 0.1 mg/ml. Approximately 1 µl sample was loaded into immersion oil in the sample holder for the osmometer, which was carefully placed onto the sample stage atop thermal paste to improve heat transfer. The sample was then frozen rapidly by lowering the temperature to -20 °C. The sample was slowly melted (~1 °C/min) until a single ice crystal (≤ 25 µm) remained. The sample was incubated for 15 min to ensure interaction of *Mp*IBP with the ice surface before the temperature was decreased at 0.01°C/min until ice growth occurred. Videos were recorded using Axiocam 506 color camera on a 1" 1.0x 60N C-mount adapter. VideoPad Video Editor (NCH Software) was used to isolate still images from video recordings.

3. Results

3.1. Primary structure of monomeric MpIBP is stable from pH 2 – pH 12

*Mp*IBP was tested for agglomeration and degradation of primary structure in varied pH solutions using SEC-MALS and BN-PAGE, which revealed that the expected protein molecular weight and monomeric state of *Mp*IBP in solution was maintained at pH 4 – pH 12, but that hydrolysis and significant degradation occurred at pH 13.

The elution time by SEC-MALS for *Mp*IBP can be related to molecular weight, indicating integrity of the primary structure. A distinct absorbance peak was observed at an elution time of 19.5 min for *Mp*IBP in pH 8 solution, the physiological control pH solution at which we expect *Mp*IBP to be intact (Fig. 1a). *Mp*IBP in solutions at pH 4, 6, and 10 expressed a peak with shape and elution time similar to *Mp*IBP at pH 8 (Fig. 1a). *Mp*IBP in pH 12 solution exhibited peak broadening, with the peak starting at ~14.5 min as opposed to 18.5 min. *Mp*IBP in pH 2 solution demonstrated a broad peak at an elution time of 20 min with a reduced intensity compared to *Mp*IBP in pH 8 solution. For *Mp*IBP in pH 2 and pH 12, it is likely that secondary or tertiary structure was disrupted (Feeney 2002) due to

changes in the protein's native charge, yielding chromatogram traces with broadened peaks compared to the native protein due to ionic interactions with the column (Barth 1998; Dil 1990). *Mp*IBP in pH 2 may have succumbed to acid mediated hydrolysis (Williams 2003), given the reduced intensity and peak broadening observed in the MALS. *Mp*IBP at pH 13 did not evince any peaks, indicating *Mp*IBP did not retain primary structure in this condition.

To verify primary structure integrity, BN-PAGE was performed (Fig. 1b). A clear band for *Mp*IBP at the expected molecular weight was seen in solutions at pH 2 to pH 12, indicating intact primary protein structure. While the predicted molecular weight of *Mp*IBP is 34 kDa, the observed band lies at a higher molecular weight. It is anticipated that the increase in observed molecular weight is likely due to a lack of complete denaturation of the protein, possibly due to calcium stabilization, and was observed in preceding literature (Garnham 2008). BN-PAGE bands were distinctly absent for *Mp*IBP at pH 13. As there was residual dye in the lanes from running the BN-PAGE, SDS-PAGE was run in addition to verify that there were no smaller protein fragments that may have been obscured by the lane run-off (Fig. S2). Only *Mp*IBP at pH 13 exhibited protein bands at lower molecular weights. The lack of a band near 34 kDa and presence of lower bands for *Mp*IBP at pH 13 corroborates the SEC-MALS result, indicating that *Mp*IBP degraded in pH 13 solution, likely due to hydrolysis of amino acids (Lawrence 1951; Radzicka 1996; Williams 2003).

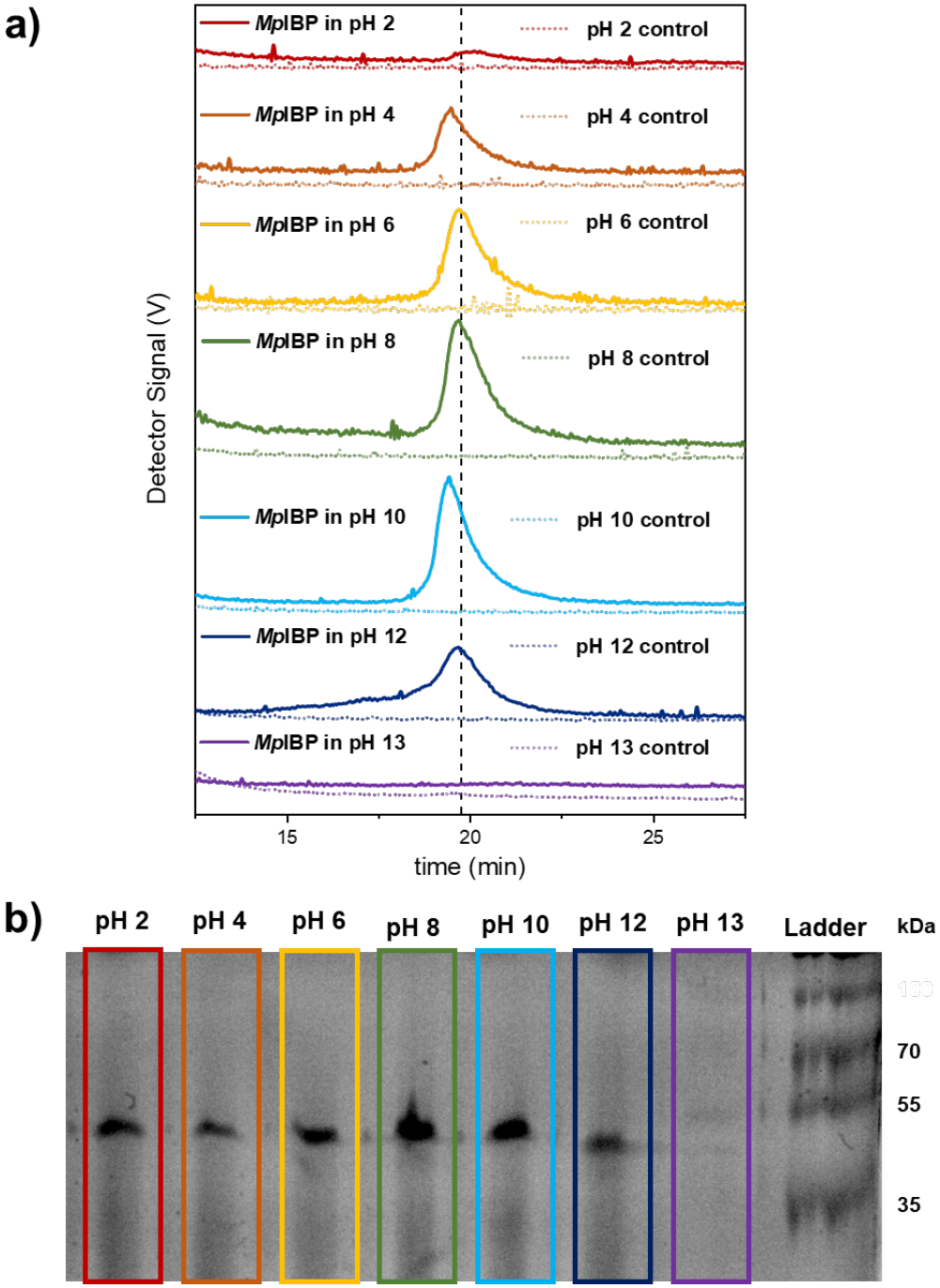

Fig. 1 The stability of *Mp*IBP in pH solutions. (a) SEC-MALS detector absorbance as a function of elution time for 1 mg/ml *Mp*IBP in solutions with pH 2 – 13. (b) BN-PAGE (10% w/v) analysis of 0.4 mg/ml *Mp*IBP stability in solutions with pH 2 – pH 13

3.2. MpIBP retains secondary structure between pH 6 and pH 10

*Mp*IBP exhibits regularly spaced β-strands that form a β-solenoid. The spacing of the ice-binding residues on the regularly spaced β-strands is currently hypothesized to contribute to its ice-binding activity (Garnham 2008; Guo 2012). Therefore, *Mp*IBP was tested for retention of secondary structure in non-physiological pH solutions using CD (Fig. 2). Data analysis using BeStSel software

parsed secondary structure of *Mp*IBP into eight categories—regular α-helix, distorted α-helix, left β-strand, relaxed β-strand, right β-strand, parallel β-strand, turn, and other (disordered) (Table 2).

As expected, ellipticity for *Mp*IBP in the pH 8 control solution exhibited a secondary structure with two distinct peaks: a positive band at 194.5 nm, and a negative band at 218 nm, which matches the spectra previously reported by Garnham *et al.* (2008) and are indicative of high β-strand content. The CD spectra for *Mp*IBP at pH 10 shows bands in the same locations as pH 8 with a slightly larger magnitude. *Mp*IBP CD spectra in pH 12 solution shows two negative bands at 216.5 and 204 nm. *Mp*IBP CD spectra in pH 13 solution was not able to be measured to achieve a true minimum due to the interference of the pH adjustor with the CD detector. Similar absorbance saturation occurred when measuring the control pH 13 solution due to the pH adjustors. Band shifts can be seen for *Mp*IBP in pH 2 (negative to 215 nm, positive to 190 nm), *Mp*IBP in pH 4 (negative to 221.5 nm, positive to ≤ 190 nm), and for *Mp*IBP in pH 6 (negative to 217 nm, positive to ≤ 195 nm).

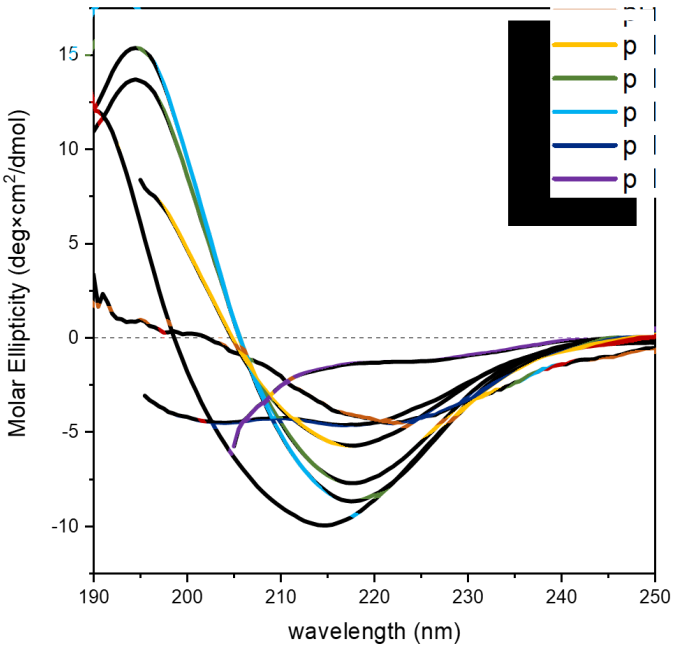

Fig. 2 The far-UV CD spectra of *Mp*IBP in the presence of varied pH solutions (pH 2 (—), pH 4 (—), pH 6 (—), pH 8 (—), pH 10 (—), pH 12 (—), pH 13 (—)). The lowest wavelength was determined by the interference of the pH adjustors and instrument absorption limits

Deconvolution of CD spectra determined that as pH deviated further from pH 8, more changes were imparted to the secondary structure of *Mp*IBP. β-strand structure is important for facilitating ice interactions, and variance the β-strand content in *Mp*IBP secondary structure (left β-strand, relaxed

β-strand, right β-strand, parallel β-strand) changed between 13.4% (pH 10) to 48.9% (pH 4) compared to *Mp*IBP in pH 8.

The protein exhibited little change in parallel β-strand content between pH 6 and pH 10, mirroring the structure determined in previous studies (Garnham 2008; Garnham 2011; Guo 2012). However, relaxed antiparallel β-strand content was lost entirely at pH 6, whereas it was prevalent at pH 8 and pH 10. At pH ≤ 4 or pH ≥ 12, the CD spectra indicated that *Mp*IBP secondary structure exhibited larger changes, especially related to β-strand structure. Although *Mp*IBP CD absorption spectra for pH 13 could not be obtained below 205 nm, the spectrum recorded indicates misfolded or unfolded protein (Kelly 2005).

Table 2 Secondary structure of *Mp*IBP under the influence of different pH solutions as determined by BeStSel software

	*Mp*IBP Structure						
Fold Type	pH 2	pH 4	pH 6	pH 8	pH 10	pH 12	*pH 13
Regular α-helix	35.0%	0.0%	6.9%	20.9%	25.6%	5.8%	-
distorted α-helix	11.9%	0.0%	5.4%	1.3%	4.0%	3.1%	-
left-twisted antiparallel β-strand	0.0%	1.8%	3.5%	4.7%	3.2%	15.5%	-
relaxed antiparallel β-strand	0.0%	0%	0.0%	16.8%	12.7%	0.0%	-
right-twisted antiparallel β-strand	14.9%	16.9%	3.1%	3.9%	0.4%	0.0%	-
parallel β-strand	11.0%	10.4%	25.2%	26.6%	30.9%	17.1%	-
turn	0.0%	39.5%	5.1%	2.1%	1.5%	7.8%	-
other (irregular/loop)	27.1%	31.5%	50.7%	23.7%	21.6%	50.8%	-

*pH 13 was not able to be measured in the minimum range for BeStSel deconvolution

3.3. MpIBP exhibits IRI activity between pH 6 and pH 12

IRI assays were implemented to determine the efficacy of *Mp*IBP to prevent ice growth in varied pH environments. As some salts have been shown to effect ice morphology (Wu 2017), control pH solutions without *Mp*IBP were compared to pH solutions with 0.1 mg/ml *Mp*IBP to rule out the influence of salt constituents. Control solutions lacking protein were used in experiments to account for effects due to changes in pH and ionic strength. As expected, all control pH solutions demonstrated ice recrystallization after incubating for 30 minutes, seen as larger ice grains compared to ice grains at t_0 (Fig. S3). All control pH solutions exhibited varied ice recrystallization end points (Fig. 3), which is expected due to the addition of pH adjusters (HCl or NaOH) that will affect the hydrogen bonding network of water based on ion interactions with the bulk, and thus affect the recrystallization process (Wu 2017, Duignan 2014). Control solutions at pH 4, pH 6, pH 10, and pH 12 have larger ice crystals at t_{30} compared to the control pH 8 solution (Fig. 3). The control pH 2 solution had the same ice recrystallization effect as the control pH 8 solution. Control pH 13 solution exhibits smaller ice crystals at t_{30} compared to control pH 8 solution, which is expected because an increase in ionic content has been shown to affect the ice recrystallization process and exhibit smaller

ice grains (Wu 2017). However, the ionic strength does not inhibit or negate the effect added IBPs (Surís-Valls 2019).

*Mp*IBP in pH 8 exhibited IRI activity, as evidenced by smaller ice grains than control pH 8 solution at t_{30} (Fig. 3). For pH 6, pH 8, pH 10, and pH 12 solutions, the addition of 0.1 mg/ml *Mp*IBP reduced the growth of ice at t_{30} compared to control pH solutions (Fig. 3, Fig. S3). For pH 4 solution, the addition of 0.1 mg/ml *Mp*IBP did not evince IRI activity and ice grain sizes at t_{30} were the same as control pH 4 solution. For pH 2 and pH 13 solutions, the addition of 0.1 mg/ml *Mp*IBP resulted in larger ice crystals as compared to control solutions. To determine if pH or ionic strength influenced *Mp*IBP activity more, ice grain sizes were estimated and normalized relative to each respective control solution. The mean largest grain size estimates were compared to pH and ionic strength (Fig. S4). It was found that pH had a greater effect on IRI than ionic strength – for example, *Mp*IBP exhibited IRI in pH 12 solution with an ionic strength of 0.078 mol/L, but did not exhibit IRI in pH 2 or pH 4 solutions, each with an ionic strength $\leq$ 0.066 mol/L.

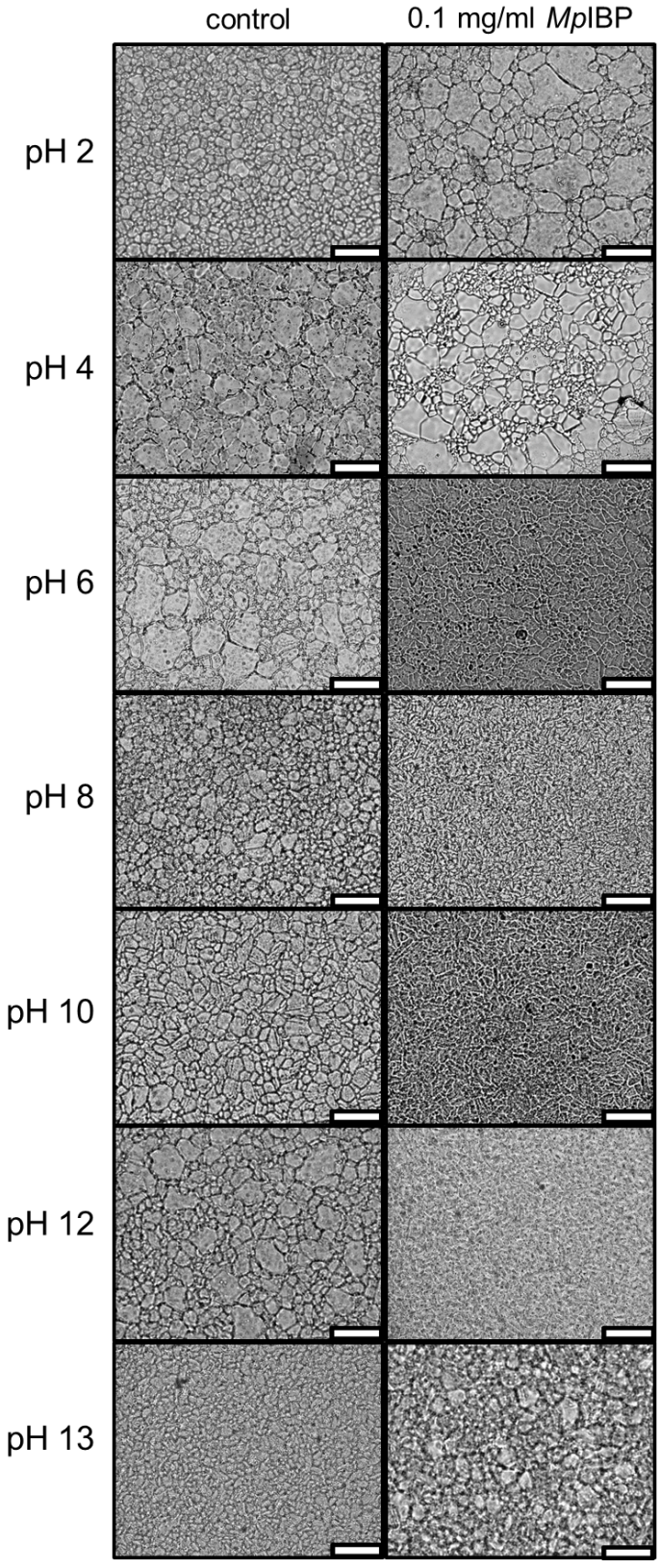

Fig. 3 IRI Micrographs at t_{30} for control pH controls (left) or for 0.1 mg/ml *Mp*IBP in non-physiological pH solutions (right)

3.4. MpIBP exhibits DIS between pH 6 and pH 10

DIS was implemented to determine if *Mp*IBP was adsorbing to the ice crystal surface (Fig. 4). None of the control pH solutions elicited dynamic ice shaping, evidenced by spherical single crystals. DIS by *Mp*IBP was readily seen in pH 6, pH 8, and pH 10 solutions as a change to hexagonal ice crystals. At pH ≥ 12 or pH ≤ 4 *Mp*IBP did not demonstrate any DIS and behaved similarly to control solutions. In physiological solutions, when *Mp*IBP adsorbs to ice crystals it prevents expansion of the crystal in the basal and prism planes, creating a hexagonal ice crystal (Garnham 2008).

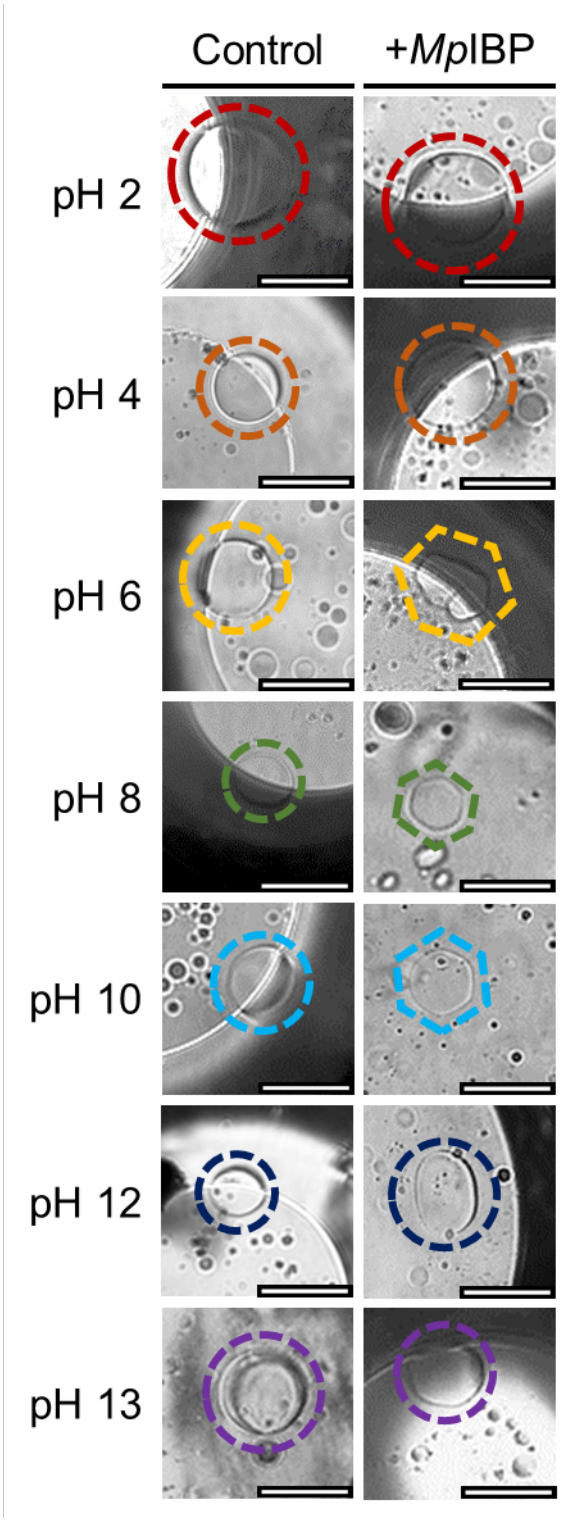

Fig. 4 Dynamic ice shaping for (left) control pH solutions and (right) 0.1 mg/ml *Mp*IBP in pH solutions. Ice crystals outlined with a circle do not demonstrate DIS, and ice crystals outlined with a hexagon demonstrate hexagonal DIS. Bubbles in the images are a result of the immersion oil. Black regions in the images are the sample holder. Scale bar = 50 μm

4. Discussion

The results displayed here demonstrate that *Mp*IBP elicits IRI activity between pH 6 – pH 12 and DIS between pH 6 – pH 10. This study investigated *Mp*IBP in various pH environments (pH 2 – pH 13). It was found that the primary structure of monomeric *Mp*IBP is stable from pH 4 – pH 12, and that secondary structure is retained between pH 6 – pH 10. To the authors' knowledge, this is one of only a few studies that looks at the IRI activity of an IBP under the influence of pH adjusted ionic solutions. Most studies investigate IRI activity in neutral ionic solutions or with added polyols, or investigate the change in thermal hysteresis activity (Amornwittawat 2008; Amornwittawat 2009; Caple 1986; Delesky 2019; Evans 2007; Kristiansen 2008; Leiter 2016; Li 1998; Surís-Valls 2019a). This novel contribution of ice inhibition by proteinaceous materials in non-physiological environments could be implemented in a variety of engineering applications.

Based on singular observable peaks in SEC-MALS and single bands at the expected molecular weight by BN-PAGE, *Mp*IBP does not aggregate or degrade in solutions between pH 4 to pH 12. *Mp*IBP only exhibits degradation in pH 13 solution, made apparent by a lack of elution peak in SEC-MALS and no prominent band at the expected molecular weight by BN-PAGE, as well as smaller molecular weight bands in SDS-PAGE. *Mp*IBP at pH 2 exhibits a broadened peak at the same elution time in SEC-MALS compared to pH 8 but exhibits a band at the expected molecular weight by BN-PAGE, suggesting intact protein with different charge interactions in the SEC-MALS column. The elution peaks for *Mp*IBP in solution with pH 4 – pH 12 are singular, and similar in size and elution time compared to *Mp*IBP in pH 8. Assuming that *Mp*IBP is monomeric at 0.1 mg/ml at pH 8 based on previous literature (Garnham 2008; Garnham 2011), it can be assumed they *Mp*IBP is also monomeric in solutions at pH 4 – pH 12. The BN-PAGE showed that the protein was not aggregating due to a lack of upper molecular weight bands, nor was it degrading due to a lack of bands at lower molecular weights, thus the primary structure of the protein is stable.

Properly folded *Mp*IBP creates a calcium-stabilized β-solenoid tertiary structure that would have its ice-binding face exposed to solution, allowing interactions with ice crystals (Fig. 5a). The β-solenoid consists of thirteen tandem repeats with the sequence -xGTGNDxuxuGGxuxGxux-, where x is any amino acid and u is a hydrophobic amino acid (Guo 2012). The current hypothesis for *Mp*IBP ice-binding activity is closely related to its regularly spaced parallel β-strands that promote a 7.4 Å spacing between ice-binding residues (threonine (T) and asparagine (N)) on the same coil of the β-solenoid, as well as 4.6 Å spacing between ice-binding resides on adjacent coils, as can be seen in Fig. 5b (Garnham 2008; Garnham 2011; Guo 2012). Oxygen atoms in the ice crystal lattice repeat at 7.37 Å along the c-axis of the primary prism plane as well as repeat at 4.52 Å along the a-axis in the

primary prism and basal planes, as can be seen in Fig. 5c. The spacing of ice-binding residues along the coils of the *Mp*IBP β-solenoid allow it to match the ice lattice on the primary prism and basal planes of ice, resulting in IRI and hexagonal DIS.

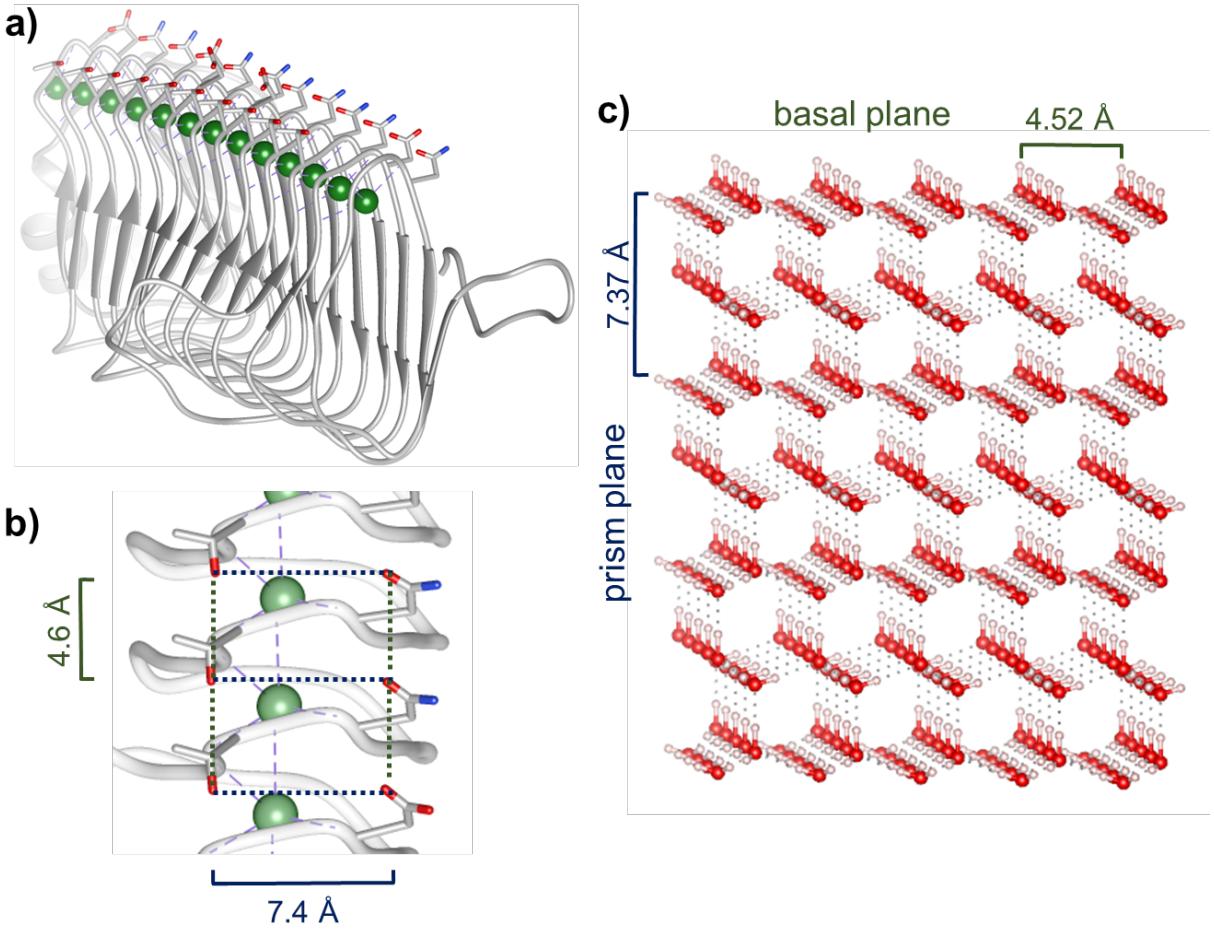

Fig. 5 (a) The β-solenoid structure of properly folded *Mp*IBP in the presence of Ca^{2+} ions (green spheres). (b) Spacing of ice-binding residues of properly folded *Mp*IBP. The ice-binding face of *Mp*IBP exhibits ice-binding residues with 7.4 Å spacing on the same coil of the β-solenoid, as well as 4.6 Å spacing between ice-binding resides on adjacent coils. (c) Schematic of the hexagonal ice crystal lattice. Oxygen atoms in the ice crystal lattice repeat at 7.35 Å along the c-axis of the primary prism plane as well as repeat at 4.52 Å along the a-axis in the primary prism plane and basal plane. *Mp*IBP crystal structure was provided by Garnham et al. (2011; PDB 3P4G). *Mp*IBP molecular graphics performed with UCSF Chimera, developed by the Resource for Biocomputing, Visualization, and Informatics at the University of California, San Francisco, with support from NIH P41-GM103311 (Pettersen 2004). Ice lattice schematic was made using VESTA software (Momma 2011)

A disruption of protein tertiary structure does not necessarily equate to loss of functionality (Ptitsyn 1987). Small molecule peptide analogs have shown activity, albeit reduced, when compared to their structured counterparts (Surís-Valls 2019b), indicating that if a portion of the protein responsible for ice growth inhibition remains intact, then some activity may be seen. Herein, CD was utilized to hypothesize how changes in secondary structure influenced IRI and DIS activity. CD

analysis revealed that *Mp*IBP exhibited relatively well folded structure between pH 8 and pH 10, consisting largely of β-strands, similar to literature precedence (Garnham 2008; Garnham 2011; Guo 2012). For *Mp*IBP in pH 10, a change of 23.5% secondary structure, taken as the absolute difference between fold types, is observed although no singular fold type changed by > 5% (Table 2), indicating *Mp*IBP stability at pH 10. Based on high IRI activity (Fig. 3) and hexagonal DIS for *Mp*IBP in pH 8 and pH 10 solutions, we suggest that the β-helix region hypothesized to interact with ice is intact (Fig. 5a) and can interact with ice crystals to reduce recrystallization (Fig. 3) or alter ice morphology (Fig. 4). Control pH 10 solution exhibited larger grain sizes than control pH 8 solution, demonstrating that for applications in pH 10 environments the crystal expansion would be more detrimental. As the control solution grain size at t_{30} was larger than pH 8 control solution, *Mp*IBP at pH 10 appeared to have the greatest reduction of ice size. Since the grain size at t_{30} for *Mp*IBP at pH 10 was similar to *Mp*IBP in pH 8 solution, it could be concluded that *Mp*IBP was most effective in pH 10 solution.

*Mp*IBP exhibited promising activity for acidic (pH 6) and basic (pH 12) solutions as a reduction of grain size was observed compared to control solutions, especially considering the final ice grain size for control solutions were larger than control pH 8 solution. *Mp*IBP in pH 6 had a greater reduction of ice size compared to *Mp*IBP in pH 8 at t_{30}. *Mp*IBP in pH 12 demonstrated a reduction of ice crystal size at t_{30} compared to control pH 12 solution. However, the crystal size for *Mp*IBP in pH 6 and pH 12 at t_{30} was larger than pH 8, indicating decreased IRI activity. The CD spectra for *Mp*IBP in pH 6 demonstrates some folded structure (Fig. 2); however, the BeStSel deconvolution (Table 2) resulted in 50% unfolded structure. *Mp*IBP exhibits a few α-helices and antiparallel β-strands that are not calcium stabilized (Fig. 5a), and it is anticipated that at pH 6 the non-stabilized structures of the protein are beginning to denature while the calcium-stabilized parallel β-strands remain intact. Similar to *Mp*IBP in pH 6, *Mp*IBP in pH 12 solution shows a decrease in secondary structure that is not calcium stabilized while retaining some parallel β-strand structure. As the ice-binding residues of *Mp*IBP are regularly spaced between the calcium-stabilized parallel β-strands (Garnham 2011), the retention of the β-strand structure could explain the of IRI activity despite the increase of irregular structure at pH 6. To further probe *Mp*IBP structure under the influence of external stressors such as pH, NMR could be implemented; however, NMR fell outside the scope of this research study.

DIS was only seen in pH 6 and pH 10 solutions where *Mp*IBP showed ≤ 5% change of parallel β-strand structure compared to pH 8, likely because the ice-binding residues still mimicked the distance of oxygen atoms in the ice lattice to facilitate adsorption (Fig. 5). The tertiary structure of *Mp*IBP regularly aligns the ice-binding residues into a 7.4 Å by 4.6 Å motif that facilitates adsorption to hexagonal ice. The 7.4 Å by 4.6 Å motif is structured through the parallel β-strands, and it is anticipated that changes in the β-strand alignment would disrupt the spacing of the residues, reducing the match to the ice crystal lattice. *Mp*IBP in pH 12 retained a similar amount of overall β-strand structure as *Mp*IBP in pH 6. However, *Mp*IBP in pH 12 retained less parallel β-strand and exhibited more twisted β-strand structure. We hypothesize that the increase of twisted β-strand is responsible

for the loss of DIS activity as there are no longer enough adjacent coils on the β-solenoid to align the ice-binding residues with an appropriate spacing to match the ice crystal lattice, but the overall retention of general β-strands resulted in IRI activity. As IRI is more reliant on the disruption of water molecules at the ice-water interface between ice grains, retention of any β-strand structure could enable some short-range water ordering to inhibit ice growth. DIS appeared to be more reliant on tertiary structure than IRI, indicating that there is a minimum amount of native structure required to ensure interaction between the protein and ice (Davies 2014). To better understand how *Mp*IBP can elicit IRI but not DIS in pH 12 solution, it could be beneficial to observe *Mp*IBP in physiological and stressed environments using neutron reflection to determine interactions at the ice-water interface (Xu 2008).

Similar to *Mp*IBP in pH 12, the secondary structure of *Mp*IBP at pH 4 showed an increase in twisted antiparallel β-strands; although *Mp*IBP in pH 4 showed right twisted antiparallel β-strands as opposed to left twisted antiparallel β-strands. However, *Mp*IBP at pH 4 did not evince any IRI activity. It is possible that the difference in the twist direction impacts the difference in IRI activity. Since *Mp*IBP has an isoelectric point of 4.1 (Table S1), *Mp*IBP was expected to exhibit instability in pH 4 solution, which resulted in measurement fluctuations in the CD detector (Xia 2018). It is possible that in pH 4 solution *Mp*IBP is unable to interact with ice due to the net neutral charge of the protein. In the future, to better understand *Mp*IBPs activity around the isoelectric point, solutions with finer gradations of pH could be implemented to glean what might be happening.

Although *Mp*IBP exhibited larger ice crystals compared to control solutions for pH 2 and pH 13, an additional class of proteins, called ice nucleation proteins, can be useful for targeting specific ice crystal sizes in solution (Bar-Dolev 2016b). The shift of CD spectra to lower wavelengths for *Mp*IBP in pH 2 solution indicates some restructuring with an increase in regular and distorted α-helix structure at the expense of turns, antiparallel β-strands, and parallel β-strands. What β-strand structure that was preserved in *Mp*IBP at pH 2 is again possibly due to calcium-stabilization and likely allowed some ice-binding residues to remain exposed to solution. For *Mp*IBP at pH 13, the amount of NaOH necessary to create a pH 13 environment caused absorbance saturation in the CD detector, preventing enough data to be collected for BeStSel deconvolution; however, the spectra that was able to be collected is reminiscent of a typical denatured protein, which is further supported by the lack of elution peak in SEC-MALS and the lack of band at the expected molecular weight by BN-PAGE, indicating protein degradation. It is possible that despite degradation some of the ice-binding residues remained intact on one or more of the sequence repeats (-xGTGNDxuxuGGxuxGxux-). Therefore, it is possible that there were enough ice-binding residues exposed to solution at pH 2 and pH 13 to interact with ice; however, without a regular structure to promote ice growth inhibition, they could facilitate ice nucleation. Ice nucleation proteins typically exhibit a common contiguous octapeptide repeat composed of mainly hydrophilic residues (-AGYGSTLT-) (Kawahara 2017). While *Mp*IPBP does not exhibit more than two adjacent residues from this octapeptide (Fig. S5), there is a -GTG-

repeat close to the -GYG- repeat, as well as a high percentage of the hydrophilic residues present in the *Mp*IBP sequence, e.g., 8.2% A, 13.9% G, and 5.7% T (Table S1). To further probe this phenomenon, it would be beneficial to investigate *Mp*IBP in pH 2 and pH 13 as a possible ice nucleator using an ice nucleation assay as described by Congdon et al. (2015). Additionally, the sequence of the protein fragments observed at pH 13 could be investigated through mass spectrometry, facilitating understanding of retained amino acid sequences capable of ice nucleation.

To contextualize the importance of investigating ice growth in extreme pH environments, previous research has shown that IRI active materials can decrease freeze-thaw damage in cement due to, in part, to prevention of ice crystal expansion (Frazier 2020; Qu 2019). Cementitious materials have a pH of 12-13 due to the presence of $Ca(OH)_2$ that creates a calcium-silicate-hydrate gel, giving concrete its strength (Ghods 2009) which necessitates pH compatible IRI additives. As Ca^{2+} plays an important role in *Mp*IBP structure, the calcium present in cementitious environments could be advantageous for an *Mp*IBP additive. Additionally, since *Mp*IBP prevents ice growth *via* IRI at pH 12, it could be a beneficial additive to cementitious environments to prevent freeze-thaw damage.

*Mp*IBP exhibits IRI activity in solutions $6 \leq pH \leq 12$, indicating that *Mp*IBP (and other IBPs) could be effective at mitigating frost-induced damage in applications that necessitate activity in somewhat non-physiological chemical environments. Although the presence of Na^+ and Ca^{2+} have been shown to effect ice crystal shape and recrystallization (Wu 2017), no shaping or significant inhibition of ice recrystallization was seen in control solutions pH 6 – 10, indication that the addition of 0.1 mg/ml *Mp*IBP affected both crystal size (Fig. 3) and shape (Fig. 4). *Mp*IBP is more resistant to the presence of OH^- compared to H_3O^+, which is substantiated by the isoelectric point of the protein ($pI \approx 4.1$). Given that *Mp*IBP is only effective at preventing ice growth in solutions $6 \leq pH \leq 12$, alternative materials for controlling ice morphology in environments beyond these pH bounds must be considered. To further improve pH stability, synthetic biology approaches could be utilized to engineer a more stable protein that retains activity and mitigates ice growth in environments with a $pH < 6$ or a $pH > 12$ (Alegre-Cebollada 2010; Hagan 2010; Kang 2007; Kang 2009; Zakeri 2015). Additionally, synthetic polymer architectures that mimic the ice-binding functionality of IBPs offer a unique avenue for mitigating and controlling ice nucleation and growth, as they may be not only more cost-effective, but also more able to inhibit ice crystal recrystallization in aggressive chemical solutions without relying on tertiary structure to elicit ice interaction activity (Biggs 2017; Congdon 2013; Congdon 2015; He 2018; Mitchell 2014; Mitchell 2015; Stubbs 2019).

5. Conclusions

This study evaluated the potential of a calcium dependent ice-binding protein (IBP) from *Marinomonas primoryensis* (*Mp*IBP) to inhibit and control ice crystal nucleation and growth in non-physiological environments, and changes in activity were found to be a function of protein structure. *Mp*IBP showed the ability to retain its primary and secondary structure in the pH range of 6

– 10 as indicated by similar CD spectra, a single elution peak in SEC-MALS, and a single band at the expected molecular weight by BN-PAGE. DIS and IRI were observed between pH 6 and pH 10. *Mp*IBP lost parallel β-strand structure at solutions of pH < 6 or pH > 10, as well as the ability to inhibit ice crystal growth and exhibit dynamic ice shaping (DIS). *Mp*IBP at pH 12 was an exception, as it misfolded but still retained IRI activity, though it did not elicit DIS. In the most extreme environments (pH 2 and pH 13), the addition of *Mp*IBP resulted in larger ice crystals after 30 min compared to control solutions. Some applications, such as preventing freeze-thaw damage in cement, require pH resilience for IRI active materials due to a highly alkaline environment (pH 12 – 13). In conclusion, these results suggest that *Mp*IBP has some applications in non-physiological environments as frost-prevention materials.

Supplementary Materials: The following are available online at www.mdpi.com/xxx/s1, Table S1: Breakdown of the structure and properties for region IV of the ice-binding protein from *Marinomonas primoryensis* (*Mp*IBP) as determined by Expasy, Table S2: Absorbance for *Mp*IBP in pH 4 solution, Table S3: Solution recipes for buffers used during *Mp*IBP purification, Fig. S1: SDS-PAGE (10% w/v) analysis of *Mp*IBP purification, Fig. S2: SDS-PAGE for *Mp*IBP in different pH solutions from Table 1 to verify that *Mp*IBP did not degrade, Fig. S3: Ice recrystallization micrographs of varied pH solutions at t_0 and t_{30} either as controls or loaded with 0.1 mg/ml *Mp*IBP, Fig. S4: Quantitative comparison of IRI activity as a function of pH or ionic strength, Fig. S5: Amino acid sequence for the ice-binding region IV from the *Marinomonas primoryensis* protein.

Author Contributions: Data curation: [Elizabeth A. Delesky]; formal analysis: [Elizabeth A. Delesky], [Patrick E. Thomas], and [Marimikel Charrier]; funding acquisition: [Wil V. Srubar III]; investigation: [Elizabeth A. Delesky] and [Patrick E. Thomas]; methodology: [Elizabeth A. Delesky], [Patrick E. Thomas], [Jeffrey C. Cameron], and [Wil V. Srubar III]; supervision: [Jeffrey C. Cameron] and [Wil V. Srubar III]; writing–original draft, [Elizabeth A. Delesky]; writing–review & editing, [Patrick E. Thomas], [Marimikel Charrier], [Jeffrey C. Cameron] and [Wil V. Srubar III]. All authors have read and agreed to the published version of the manuscript.

Funding: This research was funded by the United States (US) National Science Foundation (Award No. CMMI-1727788), the National Science Foundation Graduate Research Fellowship Program, the National Highway's Cooperative Research Program (NCHRP) (Award No. NCHRP-204), and the NIH/CU Molecular Biophysics Training Program (P.E.T.). This work represents the views of the authors and not necessarily those of the sponsors.

Acknowledgments: This research was made possible by the Department of Civil, Environmental, and Architectural Engineering, the College of Engineering and Applied Sciences, and the Living

Materials Lab at the University of Colorado Boulder. Thanks to Peter Davies at Queen's University for the gift of the *Marinomonas primoryensus* clones used in this study. A special thanks is given to Dr. Annette Erbse and the Biochemistry Shared Instruments Pool for assistance with CD Spectrometry.

Conflicts of Interest: The authors declare no conflict of interest. The funders had no role in the design of the study; in the collection, analyses, or interpretation of data; in the writing of the manuscript, or in the decision to publish the results.

5. References

Alegre-Cebollada, J., Badilla, C. L., & Fernández, J. M. (2010). Isopeptide bonds block the mechanical extension of pili in pathogenic Streptococcus pyogenes. *Journal of Biological Chemistry*, *285*(15), 11235-11242.

Amornwittawat, N., Wang, S., Banatlao, J., Chung, M., Velasco, E., Duman, J. G., & Wen, X. (2009). Effects of polyhydroxy compounds on beetle antifreeze protein activity. *Biochimica et Biophysica Acta (BBA)-Proteins and Proteomics*, *1794*(2), 341-346.

Amornwittawat, N., Wang, S., Duman, J. G., & Wen, X. (2008). Polycarboxylates enhance beetle antifreeze protein activity. *Biochimica et Biophysica Acta (BBA)-Proteins and Proteomics*, *1784*(12), 1942-1948.

Bar-Dolev, M., Celik, Y., Wettlaufer, J. S., Davies, P. L., & Braslavsky, I. (2012). New insights into ice growth and melting modifications by antifreeze proteins. *Journal of the Royal Society Interface*, *9*(77), 3249-3259.

Bar-Dolev, M., Bernheim, R., Guo, S., Davies, P. L., & Braslavsky, I. (2016). Putting life on ice: bacteria that bind to frozen water. *Journal of the Royal Society Interface*, *13*(121), 20160210.

Dolev, M. B., Braslavsky, I., & Davies, P. L. (2016). Ice-binding proteins and their function. *Annual review of biochemistry*, *85*.

Barth, H. G., Boyes, B. E., & Jackson, C. (1998). Size exclusion chromatography and related separation techniques. *Analytical chemistry*, 70(12), 251-278.

Biggs, C. I., Bailey, T. L., Graham, B., Stubbs, C., Fayter, A., & Gibson, M. I. (2017). Polymer mimics of biomacromolecular antifreezes. *Nature communications*, *8*(1), 1-12.

Buck, R. P., Singhadeja, S., & Rogers, L. B. (1954). Ultraviolet absorption spectra of some inorganic ions in aqueous solutions. *Analytical Chemistry*, *26*(7), 1240-1242.

Caple, G., Kerr, W. L., Burcham, T. S., Osuga, D. T., Yeh, Y., & Feeney, R. E. (1986). Superadditive effects in mixtures of fish antifreeze glycoproteins and polyalcohols or surfactants. *Journal of colloid and interface science*, *111*(2), 299-304.

Chao, H., DeLuca, C. I., Davies, P. L., Sykes, B. D., & Sönnichsen, F. D. (1994). Structure-function relationship in the globular type III antifreeze protein: identification of a cluster of surface residues required for binding to ice. *Protein Science*, *3*(10), 1760-1769.

Congdon, T., Dean, B. T., Kasperczak-Wright, J., Biggs, C. I., Notman, R., & Gibson, M. I. (2015). Probing the biomimetic ice nucleation inhibition activity of poly (vinyl alcohol) and comparison to synthetic and biological polymers. *Biomacromolecules*, *16*(9), 2820-2826.

Congdon, T., Notman, R., & Gibson, M. I. (2013). Antifreeze (glyco) protein mimetic behavior of poly (vinyl alcohol): detailed structure ice recrystallization inhibition activity study. *Biomacromolecules*, *14*(5), 1578-1586.

Davies, P. L. (2014). Ice-binding proteins: a remarkable diversity of structures for stopping and starting ice growth. *Trends in biochemical sciences*, *39*(11), 548-555.

Davies, P. L., Hew, C. L., & Fletcher, G. L. (1988). Fish antifreeze proteins: physiology and evolutionary biology. *Canadian Journal of Zoology*, *66*(12), 2611-2617.

Delesky, E. A., Frazier, S. D., Wallat, J. D., Bannister, K. L., Heveran, C. M., & Srubar, W. V. (2019). Ice-Binding Protein from Shewanella frigidimarinas Inhibits Ice Crystal Growth in Highly Alkaline Solutions. *Polymers*, *11*(2), 299.

DeVries, A. L. (1988). The role of antifreeze glycopeptides and peptides in the freezing avoidance of Antarctic fishes. *Comparative Biochemistry and Physiology Part B: Comparative Biochemistry*, *90*(3), 611-621.

Dill, K. A. (1990). Dominant forces in protein folding. *Biochemistry*, *29*(31), 7133-7155.

Duignan, T. T., Parsons, D. F., & Ninham, B. W. (2014). Collins's rule, Hofmeister effects and ionic dispersion interactions. *Chemical physics letters*, *608*, 55-59.

Duman, J. G., & Olsen, T. M. (1993). Thermal hysteresis protein activity in bacteria, fungi, and phylogenetically diverse plants. *Cryobiology*, *30*(3), 322-328.

Evans, R. P., Hobbs, R. S., Goddard, S. V., & Fletcher, G. L. (2007). The importance of dissolved salts to the in vivo efficacy of antifreeze proteins. *Comparative Biochemistry and Physiology Part A: Molecular & Integrative Physiology*, *148*(3), 556-561.

Feeney, E. P., Guinee, T. P., & Fox, P. F. (2002). Effect of pH and calcium concentration on proteolysis in Mozzarella cheese. *Journal of Dairy science*, *85*(7), 1646-1654.

Fiala, G. J., Schamel, W. W., & Blumenthal, B. (2011). Blue native polyacrylamide gel electrophoresis (BN-PAGE) for analysis of multiprotein complexes from cellular lysates. *JoVE (Journal of Visualized Experiments)*, (48), e2164.

Fletcher, G. L., King, M. J., & Kao, M. H. (1987). Low temperature regulation of antifreeze glycopeptide levels in Atlantic cod (Gadus morhua). *Canadian journal of zoology*, *65*(2), 227-233.

Frazier, S. D., Matar, M. G., Osio-Norgaard, J., Aday, A. N., Delesky, E. A., & Srubar III, W. V. (2020). Inhibiting Freeze-Thaw Damage in Cement Paste and Concrete by Mimicking Nature's Antifreeze. *Cell Reports Physical Science*, 100060.

Garnham, C. P., Campbell, R. L., & Davies, P. L. (2011). Anchored clathrate waters bind antifreeze proteins to ice. *Proceedings of the National Academy of Sciences*, *108*(18), 7363-7367.

Garnham, C. P., Gilbert, J. A., Hartman, C. P., Campbell, R. L., Laybourn-Parry, J., & Davies, P. L. (2008). A Ca2+-dependent bacterial antifreeze protein domain has a novel β-helical ice-binding fold. *Biochemical Journal*, *411*(1), 171-180.

Gauthier, S. Y., Kay, C. M., Sykes, B. D., Walker, V. K., & Davies, P. L. (1998). Disulfide bond mapping and structural characterization of spruce budworm antifreeze protein. *European journal of biochemistry*, *258*(2), 445-453.

Ghods, P., Isgor, O. B., McRae, G., & Miller, T. (2009). The effect of concrete pore solution composition on the quality of passive oxide films on black steel reinforcement. *Cement and Concrete Composites*, *31*(1), 2-11.

Gilbert, J. A., Hill, P. J., Dodd, C. E., & Laybourn-Parry, J. (2004). Demonstration of antifreeze protein activity in Antarctic lake bacteria. *Microbiology*, *150*(1), 171-180.

Graether, S. P., Kuiper, M. J., Gagné, S. M., Walker, V. K., Jia, Z., Sykes, B. D., & Davies, P. L. (2000). β-Helix structure and ice-binding properties of a hyperactive antifreeze protein from an insect. *Nature*, *406*(6793), 325-328.

Graham, L. A., & Davies, P. L. (2005). Glycine-rich antifreeze proteins from snow fleas. *Science*, *310*(5747), 461-461.

Griffith, M., Ala, P., Yang, D. S., Hon, W. C., & Moffatt, B. A. (1992). Antifreeze protein produced endogenously in winter rye leaves. *Plant Physiology*, *100*(2), 593-596.

Guo, S., Garnham, C. P., Whitney, J. C., Graham, L. A., & Davies, P. L. (2012). Re-evaluation of a bacterial antifreeze protein as an adhesin with ice-binding activity. *PloS one*, *7*(11).

Hagan, R. M., Björnsson, R., McMahon, S. A., Schomburg, B., Braithwaite, V., Bühl, M., ... & Schwarz-Linek, U. (2010). NMR spectroscopic and theoretical analysis of a spontaneously formed Lys–Asp isopeptide bond. *Angewandte Chemie International Edition*, *49*(45), 8421-8425.

He, Z., Liu, K., & Wang, J. (2018). Bioinspired materials for controlling ice nucleation, growth, and recrystallization. *Accounts of chemical research*, *51*(5), 1082-1091.

Hew, C. L., Slaughter, D., Fletcher, G. L., & Joshi, S. B. (1981). Antifreeze glycoproteins in the plasma of Newfoundland Atlantic cod (Gadus morhua). *Canadian Journal of Zoology*, *59*(11), 2186-2192.

Hoshino, T., Kiriaki, M., Ohgiya, S., Fujiwara, M., Kondo, H., Nishimiya, Y., ... & Tsuda, S. (2003). Antifreeze proteins from snow mold fungi. *Canadian Journal of Botany*, *81*(12), 1175-1181.

Jia, Z., DeLuca, C. I., Chao, H., & Davies, P. L. (1996). Structural basis for the binding of a globular antifreeze protein to ice. *Nature*, *384*(6606), 285-288.

Kang, H. J., & Baker, E. N. (2009). Intramolecular isopeptide bonds give thermodynamic and proteolytic stability to the major pilin protein of Streptococcus pyogenes. *Journal of Biological Chemistry*, *284*(31), 20729-20737.

Kang, H. J., Coulibaly, F., Clow, F., Proft, T., & Baker, E. N. (2007). Stabilizing isopeptide bonds revealed in gram-positive bacterial pilus structure. *Science*, *318*(5856), 1625-1628.

Kawahara, H. (2017). Cryoprotectants and ice-binding proteins. In *Psychrophiles: from biodiversity to biotechnology* (pp. 237-257). Springer, Cham.

Kelly, S. M., Jess, T. J., & Price, N. C. (2005). How to study proteins by circular dichroism. *Biochimica et Biophysica Acta (BBA)-Proteins and Proteomics*, *1751*(2), 119-139.

Knight, C. A., Cheng, C. C., & DeVries, A. L. (1991). Adsorption of alpha-helical antifreeze peptides on specific ice crystal surface planes. *Biophysical journal*, *59*(2), 409-418.

Knight, C. A., Hallett, J., & DeVries, A. L. (1988). Solute effects on ice recrystallization: an assessment technique. *Cryobiology*, *25*(1), 55-60.

Krause, F., & Seelert, H. (2008). Detection and analysis of protein-protein interactions of organellar and prokaryotic proteomes by blue native and colorless native gel electrophoresis. *Current protocols in protein science*, *54*(1), 19-18.

Kristiansen, E., & Zachariassen, K. E. (2005). The mechanism by which fish antifreeze proteins cause thermal hysteresis. *Cryobiology*, *51*(3), 262-280.

Kristiansen, E., Pedersen, S. A., & Zachariassen, K. E. (2008). Salt-induced enhancement of antifreeze protein activity: a salting-out effect. *Cryobiology*, *57*(2), 122-129.

Lawrence, L., & Moore, W. J. (1951). Kinetics of the hydrolysis of simple glycine peptides. *Journal of the American Chemical Society*, *73*(8), 3973-3977.

Leiter, A., Rau, S., Winger, S., Muhle-Goll, C., Luy, B., & Gaukel, V. (2016). Influence of heating temperature, pressure and pH on recrystallization inhibition activity of antifreeze protein type III. *Journal of food engineering*, *187*, 53-61.

Li, N., Andorfer, C. A., & Duman, J. G. (1998). Enhancement of insect antifreeze protein activity by solutes of low molecular mass. *Journal of Experimental Biology*, *201*(15), 2243-2251.

Liang, S., Yuan, B., Kwon, J. W., Ahn, M., Cui, X. S., Bang, J. K., & Kim, N. H. (2016). Effect of antifreeze glycoprotein 8 supplementation during vitrification on the developmental competence of bovine oocytes. *Theriogenology*, *86*(2), 485-494.

Liou, Y. C., Thibault, P., Walker, V. K., Davies, P. L., & Graham, L. A. (1999). A complex family of highly heterogeneous and internally repetitive hyperactive antifreeze proteins from the beetle Tenebrio molitor. *Biochemistry*, *38*(35), 11415-11424.

Liou, Y. C., Tocilj, A., Davies, P. L., & Jia, Z. (2000). Mimicry of ice structure by surface hydroxyls and water of a β-helix antifreeze protein. *Nature*, *406*(6793), 322-324.

Marshall, C. B., Fletcher, G. L., & Davies, P. L. (2004). Hyperactive antifreeze protein in a fish. *Nature*, *429*(6988), 153-153.

Micsonai, A., Wien, F., Kernya, L., Lee, Y. H., Goto, Y., Réfrégiers, M., & Kardos, J. (2015). Accurate secondary structure prediction and fold recognition for circular dichroism spectroscopy. *Proceedings of the National Academy of Sciences*, *112*(24), E3095-E3103.

Middleton, A. J., Vanderbeld, B., Bredow, M., Tomalty, H., Davies, P. L., & Walker, V. K. (2014). Isolation and characterization of ice-binding proteins from higher plants. In *Plant Cold Acclimation* (pp. 255-277). Humana Press, New York, NY.

Mitchell, D. E., Cameron, N. R., & Gibson, M. I. (2015). Rational, yet simple, design and synthesis of an antifreeze-protein inspired polymer for cellular cryopreservation. *Chemical Communications*, *51*(65), 12977-12980.

Mitchell, D. E., Lilliman, M., Spain, S. G., & Gibson, M. I. (2014). Quantitative study on the antifreeze protein mimetic ice growth inhibition properties of poly (ampholytes) derived from vinyl-based polymers. *Biomaterials Science*, *2*(12), 1787-1795.

Moffatt, B., Ewart, V., & Eastman, A. (2006). Cold comfort: plant antifreeze proteins. *Physiologia Plantarum*, *126*(1), 5-16.

Momma, K., & Izumi, F. (2011). VESTA 3 for three-dimensional visualization of crystal, volumetric and morphology data. *Journal of applied crystallography*, *44*(6), 1272-1276.

Pettersen, E. F., Goddard, T. D., Huang, C. C., Couch, G. S., Greenblatt, D. M., Meng, E. C., & Ferrin, T. E. (2004). UCSF Chimera—a visualization system for exploratory research and analysis. *Journal of computational chemistry*, *25*(13), 1605-1612.

Powers, T. C. (1975). Freezing effects in concrete. *Special Publication*, *47*, 1-12.

Ptitsyn, O. B. (1987). Protein folding: hypotheses and experiments. *Journal of Protein Chemistry*, *6*(4), 273-293.

Qu, Z., Guo, S., Sproncken, C. C., Surís-Valls, R., Yu, Q., & Voets, I. K. (2019). Enhancing the Freeze–Thaw Durability of Concrete through Ice Recrystallization Inhibition by Poly (vinyl alcohol). *ACS Omega*.

Radzicka, A., & Wolfenden, R. (1996). Rates of uncatalyzed peptide bond hydrolysis in neutral solution and the transition state affinities of proteases. *Journal of the American Chemical Society*, *118*(26), 6105-6109.

Slaughter, D., Fletcher, G. L., Ananthanarayanan, V. S., & Hew, C. L. (1981). Antifreeze proteins from the sea raven, Hemitripterus americanus. Further evidence for diversity among fish polypeptide antifreezes. *Journal of Biological Chemistry*, *256*(4), 2022-2026.

Song, B., Cho, J. H., & Raleigh, D. P. (2007). Ionic-strength-dependent effects in protein folding: Analysis of rate equilibrium free-energy relationships and their interpretation. *Biochemistry*, *46*(49), 14206-14214.

Stubbs, C., Congdon, T. R., & Gibson, M. I. (2019). Photo-polymerisation and study of the ice recrystallisation inhibition of hydrophobically modified poly (vinyl pyrrolidone) co-polymers. *European Polymer Journal*, *110*, 330-336.

Surís-Valls, R., & Voets, I. K. (2019). Peptidic antifreeze materials: prospects and challenges. *International journal of molecular sciences*, *20*(20), 5149.

Surís-Valls, R., & Voets, I. K. (2019). The impact of salts on the ice recrystallization inhibition activity of antifreeze (Glyco) proteins. *Biomolecules*, *9*(8), 347.

Vance, T. D., Graham, L. A., & Davies, P. L. (2018). An ice-binding and tandem beta-sandwich domain-containing protein in Shewanella frigidimarina is a potential new type of ice adhesin. *The FEBS journal*, *285*(8), 1511-1527.

Vance, T. D., Olijve, L. L., Campbell, R. L., Voets, I. K., Davies, P. L., & Guo, S. (2014). Ca2+-stabilized adhesin helps an Antarctic bacterium reach out and bind ice. *Bioscience reports*, *34*(4).

Voets, I. K. (2017). From ice-binding proteins to bio-inspired antifreeze materials. *Soft Matter*, *13*(28), 4808-4823.

Williams, A. P. (2003). Amino Acids | Determination. In *Encyclopedia of Food Sciences and Nutrition* 2nd Ed., Academic, pp. 192-197.

Wu, D. W., Duman, J. G., Cheng, C. H. C., & Castellino, F. J. (1991). Purification and characterization of antifreeze proteins from larvae of the beetle Dendroides canadensis. *Journal of Comparative Physiology B*, *161*(3), 271-278.

Wu, S., Zhu, C., He, Z., Xue, H., Fan, Q., Song, Y., ... & Wang, J. (2017). Ion-specific ice recrystallization provides a facile approach for the fabrication of porous materials. *Nature communications*, *8*, 15154.

Xia, X. (2007). Protein isoelectric point. *Bioinformatics and the Cell: Modern Computational Approaches in Genomics, Proteomics and Transcriptomics*, 207-219.

Xiao, N., Suzuki, K., Nishimiya, Y., Kondo, H., Miura, A., Tsuda, S., & Hoshino, T. (2010). Comparison of functional properties of two fungal antifreeze proteins from Antarctomyces psychrotrophicus and Typhula ishikariensis. *The FEBS journal*, *277*(2), 394-403.

Xu, H., Perumal, S., Zhao, X., Du, N., Liu, X. Y., Jia, Z., & Lu, J. R. (2008). Interfacial adsorption of antifreeze proteins: a neutron reflection study. *Biophysical journal*, *94*(11), 4405-4413.

Zakeri, B. (2015). Synthetic Biology: A New Tool for the Trade. *ChemBioChem*, *16*(16), 2277-2282.